Journal of Crystal Growth 483 (2018) 200–205

Contents lists available at ScienceDirect

Journal of Crystal Growth

journal homepage: www.elsevier.com/locate/crys

Study on growth techniques and macro defects of large-size Nd:YAG laser crystal

Jiliang Quan [a,c], Xin Yang [a], Mingming Yang [a], Decai Ma [b], Jinqiang Huang [c], Yunzhong Zhu [b,*], Biao Wang [a,b,*]

[a] State Key Laboratory of Optoelectronic Materials and Technologies/Institute of Optoelectronic and Functional Composite Materials, School of Physics and Engineering, Sun Yat-sen University, Guangzhou 510275, China
[b] Sino French Institute of Nuclear Engineering and Technology, Sun Yat-sen University, Zhuhai 519082, China
[c] Guangzhou Semiconductor Material Academy, Guangzhou 510610, China

ARTICLE INFO

Article history:
Received 29 June 2017
Received in revised form 30 November 2017
Accepted 3 December 2017
Available online 5 December 2017
Communicated by K. Jacobs

Keywords:
A2. Single crystal growth
A2. Czochralski method
A2. Large size
A1. Defects
B1. Nd:YAG
B1. Oxides

ABSTRACT

Large-size neodymium-doped yttrium aluminum garnet (Nd:YAG) single crystals were grown by the Czochralski method. The extinction ratio and wavefront distortion of the crystal were tested to determine the optical homogeneity. Moreover, under different growth conditions, the macro defects of inclusion, striations, and cracking in the as-grown Nd:YAG crystals were analyzed. Specifically, the inclusion defects were characterized using scanning electron microscopy and energy dispersive spectroscopy. The stresses of growth striations and cracking were studied via a parallel plane polariscope. These results demonstrate that improper growth parameters and temperature fields can enhance defects significantly. Thus, by adjusting the growth parameters and optimizing the thermal environment, high-optical-quality Nd:YAG crystals with a diameter of 80 mm and a total length of 400 mm have been obtained successfully.
© 2017 Elsevier B.V. All rights reserved.

1. Introduction

Because of the important role of lasers in industrial, medical, and scientific fields, the high power solid-state laser has attracted great attention [1–5]. In the past decade, the average power output of solid-state lasers has increased from 1 to 10 kW; it is even expected to reach 100 kW. However, as the core material in solid-state laser devices, the performance of laser crystals cannot meet the development needs of solid-state laser technology. Specifically, the study of large-size crystals for high power lasers has developed slowly; additionally, the optical quality of laser crystals is poor. Neodymium-doped yttrium aluminum garnet (Nd:YAG) crystals are the most commonly used active medium in high-power continuous and average power pulse solid-state lasers [6–8]. Because of its excellent properties, including optical uniformity, high gain, and the small radial concentration gradient of the Nd^{3+} ion, Nd:YAG has become the pillar material for producing high-power solid state lasers. Large-diameter Nd:YAG crystals not only meet the quality requirements of large-size laser rods and slabs, but also improve the production efficiency of a single crystal boule.

It is difficult to achieve mass production of large-size, high-quality Nd:YAG crystals due to the inaccessibility of certain growth conditions, such as high growth temperature, serious component segregation of the Nd^{3+} ion, solid solution limit, easy crack formation, and the presence of the core and lateral. Although studies on the growth of Nd:YAG crystals have been carried out for more than 40 years, there have been few reports focusing on the growth of large-diameter Nd:YAG crystals, and more attention has been bestowed upon its laser properties. Only a few studies focusing on ϕ 50 mm Nd:YAG [9], the high Nd^{3+} concentration [10], crystal defects [7,11–18], and growth simulation [19] of Nd:YAG crystals have been reported. The actual temperature field is too complicated for computer simulation; therefore, limited quantitative studies on the growth of large-size Nd:YAG crystals have been reported. Furthermore, important issues, such as suitable temperature field and optimum growth parameters, remain unsolved. The correlation studies on the growth and properties of large-size Nd:YAG laser crystals offer significant academic and economic benefit. In this paper, to solve the above issues, we studied the temperature field and growth mechanism of large-size Nd:YAG crystals. The

* Corresponding authors at: State Key Laboratory of Optoelectronic Materials and Technologies/Institute of Optoelectronic and Functional Composite Materials, School of Physics and Engineering, Sun Yat-sen University, Guangzhou 510275, China; Sino French Institute of Nuclear Engineering and Technology, Sun Yat-sen University, Zhuhai 519082, China.
E-mail addresses: zhuyzh7@mail.sysu.edu.cn (Y. Zhu), wangbiao@mail.sysu.edu.cn (B. Wang).

https://doi.org/10.1016/j.jcrysgro.2017.12.004
0022-0248/© 2017 Elsevier B.V. All rights reserved.

issues of inclusions, cracks, and other defects in the growth of crystals were addressed. Thus, Nd:YAG laser crystals of 80 mm diameter were successfully grown.

2. Materials and methods

Nd:YAG laser crystals with a doping concentration of 1 at% Nd^{+3} were grown by the conventional Czochralski (CZ) method using a radio frequency (RF) induction heater. The raw powders of Y_2O_3 (5N), Al_2O_3 (5N), and Nd_2O_3 (6N) were adequately mixed in the stoichiometric ratio, then pressed into a cylinder and calcined at 1300 °C for 24 h. An iridium crucible (180 mm diameter, 200 mm height) was chosen as the heating element. The crucible was surrounded by an isolated zirconia cylinder. Then, the multilayer zirconium oxide and ceramic materials were aligned in a double wall structure. The suitable relative height between the induction coil and the crucible was modulated to achieve a high temperature gradient and the optimal thermal field to grow large-size Nd:YAG crystals. The entire growth process was performed in argon shielding gas. During crystal growth, high precision in temperature was realized using a 2404 type Eurotherm temperature control system. The temperatures above melt (0, 5, 10 mm from the melt surface) were measured by Ir-Rh thermocouples. A computer simulation was also performed.

Next, an oriented Nd:YAG crystal was employed as the seed crystal. The raw materials in the crucible were then melted at ~1970 °C. After placing the seeds into the melt, changes in the crystallization front were monitored carefully. The suitable seeding temperature was determined after seeding down several times. This seeding temperature corresponds to the temperature at which the weight of the seed remains constant and the seed undergoes microfusion. The crystal growth program was then turned into the automatic diameter controlled (ADC) function to start body control. During the growth process, a pulling rate of 0.5–0.8 mm/h and a rotation rate of 12–18 rpm were employed.

The stress (induced by the defects) that affects the crystal quality was studied by a parallel plane polariscope (PSV-201). The extinction ratio and wavefront distortion of the as-grown crystals were studied with an extinction ratio meter (ER2000) and laser interferometer (G30D). Inclusion defects, in the transversely sliced and polished crystal cylinder, could be revealed by scanning electron microscopy (SEM). The chemical compositions of the defective area were characterized by an energy dispersive spectrometer (EDS).

3. Results and discussion

A series of defects, such as cracks, color center, inclusions, etc. often emerges during the growth of a large-diameter Nd:YAG crystal, which significantly degrades the crystal quality and limits productivity. To understand the mechanism behind the generation of these macro defects, we grew numerous Nd:YAG crystals under different growth conditions. Figs. 1–3 present the defective ones grown in the early stage of our study.

Fig. 1a shows a crystal interface that suddenly melted-off. The tail portion indicates that the crystal/melt interface tends to form a concave shape toward the melt. It is important to note that, during the growth of the as-grown crystal, the ADC system does not present any abnormal sudden weight or temperature changes. Also in Fig. 1a, obvious growth striations are observed in the region from the shoulder to the cylindrical part of the crystal. The striations and diameter variations correspond with the observed growth rate fluctuations during the growth process [20]. Moreover, as shown in Fig. 1b and c, the crystal exhibits a wide central core with high tension. These results indicate that the inducement of

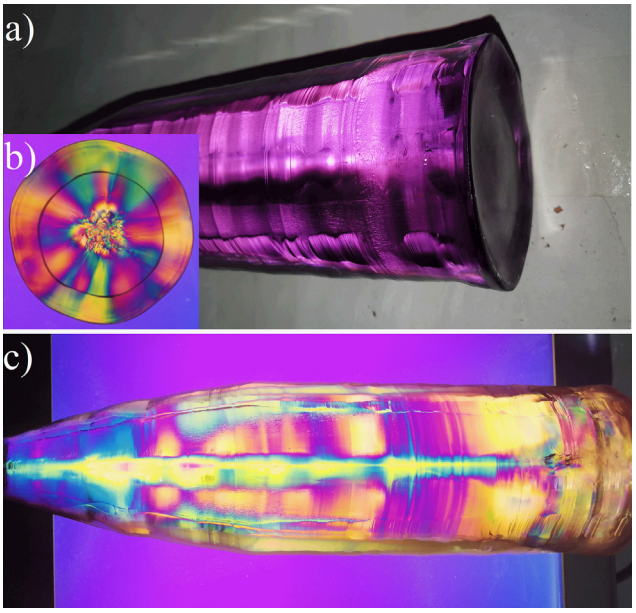

Fig. 1. (a) Nd:YAG boule which processes growth striations and the concave growth interface. (b) Longitudinal parallel-plane polariscopic image of the end face of the crystal. (c) Transverse parallel-plane polariscopic image of the crystal.

defects can be attributed to the inappropriate temperature field of the solid-liquid interface.

In the CZ method, crystal growth is initiated at the solid-liquid interface; the latent heat of crystallization is released through the solid-liquid interface as well. A variety of defects is produced when the crystal is grown in an unsuitable temperature field. Furthermore, the temperature and convection distribution determine the shape of the solid-liquid interface. Thus, a proper melt/crystal interface is important to obtain high-quality single crystals. To change the temperature distribution, we adjusted the relative vertical height between the iridium crucible and the RF coil, and decreased the insulation effect (of the thermal insulation) above the crucible to increase the temperature gradient along the growth direction. In addition to the intuitive approach of changing the thermal insulation, the crystal rotation rate also determines the convection and temperature fields of CZ melt [21]. As the crystal rotation rate increases and the vertical temperature gradient decreases, the interface shape can change from convex to concave toward the melt [21–23]. Approaching the problem from this point of view, in order to reduce the forced convection, we changed the rotation rate from 16 to 14 rpm gradually in the cylindrical part. Finally, we modulated the temperature gradient above the melt from −1 °C/mm to 25 °C/mm; the temperature gradient of the solid-liquid interface was then effectively improved.

Fig. 2a shows the different-sized and irregularly shaped inclusions inside the crystal. The polariscopic image (Fig. 2b) of the crystal exhibits a wide area comprised of a central core, inclusions, and precipitated compositions, which implies poor optical quality. In order to thoroughly examine these defects, the crystal boule was cut and polished along the ⟨1 1 1⟩ direction. Fig. 2c and d present SEM images of the polished ⟨1 1 1⟩ slice. In these figures, cloud and flake-like inclusions are observed. In Fig. 2c, positions 1 and 2 were examined using EDS to compare the composition differences between the inclusions and normal crystallization region. Table 1 illustrates the results of the EDS measurements. The primary elements of C, O, Al, and Y, and the impurity elements of Ta and Ir were found in parcel zone 1. Obviously, position 1 contains more evaporated carbon than position 2, which indicates that position 1 contains cavities. The impurities, Ta and Ir, originate

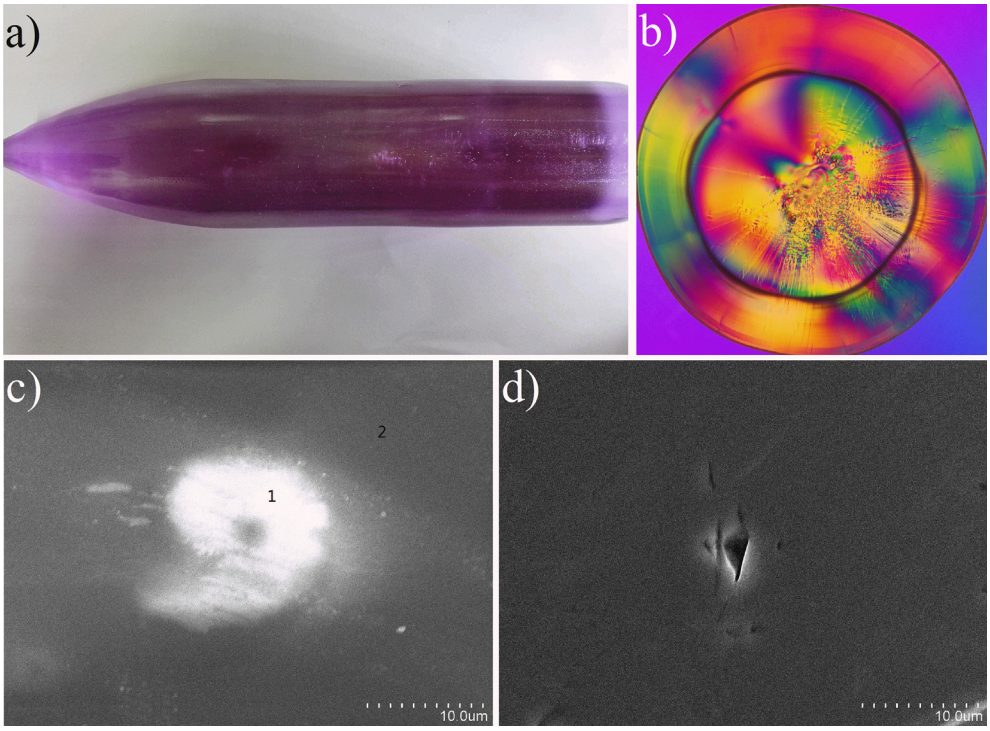

Fig. 2. (a) Illustration of inclusions in the Nd:YAG boule (b) Longitudinal parallel-plane polariscopic image of the crystal, (c) and (d) SEM images of inclusions.

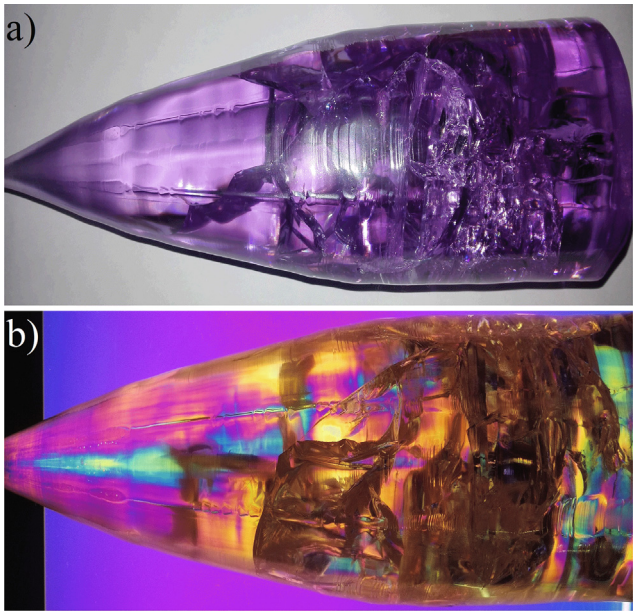

Fig. 3. (a) Fully cracked Nd:YAG shoulder and (b) the corresponding longitudinal parallel-plane polariscopic image.

from the micro impurities in the initial raw materials and the volatilization of the iridium crucible at high temperature, respectively. Comparing the normalized primary elements of positions 1 and 2, a high doping concentration of Nd^{3+} ions and impurities are found in the O defect site in position 1. A suitable Nd content is observed in the Y defect sites of position 2, which is in accordance with the segregation trend of Nd in the grown Nd:YAG crystals. Furthermore, we observe a sheet-like inclusion in Fig. 2d. This is because the Ir element is volatile at high temperatures; in the crucible, small Ir chips are easily formed into the solid-liquid interface (especially the shoulder and tail of the crystal). Our discussion is consistent with the EDS analysis as well.

In the Nd:YAG crystal, since the radius of Nd^{3+} (1.323 Å) is 10% larger than that of Y^{3+} (1.281 Å), and owing to the space sequence effect, the Nd^{3+} ions partly replace the Y^{3+} sites [11]. Moreover, the segregation coefficient of Nd^{3+} in the YAG melt is maintained around $k = 0.2$ [24]. This means, as the crystal growth occurs, the concentration of Nd^{3+} ions increases in the melt. This concentration enrichment could induce a decrease in the freezing point. This corresponds to the Nd^{3+} constitutional supercooling phenomenon [12]. The stable planar interface is destroyed after the emergence of supercooling and transforms into a cellular interface. The solute concentration of the melt then fills into the grooves of the cellular interface. Then, the solution with a high concentration and low freezing point would be enclosed in the crystal; the inclusion defects, such as clouds and cavities would be formed in the crystal. In order to overcome the supercooling of components, a larger temperature gradient (axial component) is necessary. However, an excessively large temperature gradient should also be avoided since it could lead to cracking, high stress, and dislocation [10]. Therefore, we used a multilayer insulation system to reduce the temperature gradient above the melt (also mentioned in the next

Table 1
EDS analysis of atom percentage composition in the Nd:YAG crystal.

Element	C	O	Al	Y	Nd	Ta	Ir
Position1	32.39	37.91	16.32	11.76	0.23	0.85	0.54
Position2	18.04	52.38	17.37	12.06	0.15	0	0

section). The thermal insulation system on the crucible was modified to change the temperature distribution. Thus, the supercooling phenomenon of the component could be restricted effectively.

In addition to inclusions, cracking easily occurs in large-diameter Nd:YAG crystals. Fig. 3a shows the comminuted cracking that occurs during the process of shoulder expansion. The polariscopic result, as shown in Fig. 3b, illustrates that the crystal possesses high tension. It is well known that the crystallization speed increases with the expansion of the diameter and causes an increase in stress inside the crystal. The cracking phenomenon occurs especially easily during the process of crystal shoulder growth when the stress in the crystal exceeds its yield force. Brice [18] proposed an approximation formula to describe the maximum axial temperature gradient at which no cracking occurs:

$$\left(\frac{\partial T}{\partial_z}\right)_{\max} = \left(\frac{2}{h}\right)^{1/2}\left(\frac{2\varepsilon}{\alpha R^{1.5}}\right) \quad (1)$$

where ε is the fracture strain value, α is the thermal expansion coefficient, and h is the heat transfer coefficient. From Eq. (1), the maximum axial temperature gradient of the growth crystal is approximately inversely proportional to $R^{1.5}$. Therefore, the axial gradient must be reduced to prevent the cracking of the Nd:YAG crystals. This means that the axial temperature gradient should be decreased as the diameter of the crystal is increased. Approaching the problem from this point of view, we used a multilayer thermal insulation device above the crucible; the axial temperature gradient above the melt was reduced from 35 °C/mm to 25 °C/mm. The cone angle was also changed from 45° to 30° to reduce the thermal stress in the shoulder part.

Fig. 4a shows the temperature distribution of the melt surface of the above three types of defective crystals and the modified one. More specifically, the optimized temperature field refers to TF_1 (temperature field one); and TF_2, TF_3, and TF_4 correspond to the temperature field profiles of the as-grown crystals shown in Figs. 1–3, respectively. The experimental results indicate that the temperature gradient above the melt of about 25 °C/mm can yield a high-quality Nd:YAG crystal. The results of temperature field adjustment have also been confirmed by computer simulation. Fig. 4b and c show the simulation results of the poor and the modified temperature field. Fig. 4b and c contain the schematic diagram of the insulation system before and after the adjustment, respectively. The simulation results are very similar to the actual situation of the crystal. Specifically, the temperature gradient above Fig. 4b is small, resulting in a concave crystal interface. Thus, we adjusted the insulation system, as shown in Fig. 4c, to enhance the above temperature gradient and obtain an ideal growth interface. The specific crystal appearance and performance will be presented in the following section.

In addition to the temperature field during crystal growth, as observed in our previous experiments, the tail of the crystal often exhibits a cracking phenomenon in the cooling process. Fig. 5a shows the sudden appearance of cracks with the exponentially increasing cooling rate. The corresponding polariscopic images (Fig. 5b) of the crystal illustrate a high tension in the tail part. During the crystal cooling process, thermal stresses and associated strains build up, resulting in the release of stress cracks the crystal [25]. From this, we conclude that the fast cooling rate generates a large heat stress in the tail of the crystal. Therefore, we adopted a multi-stage moderate cooling program (illustrated in Fig. 5c) to reduce the convection from the cold and hot atmosphere in the growth chamber, and to maintain a suitable temperature gradient in the furnace. This measure could overcome the occurrence of cracking. Thus, Nd:YAG crystals without cracking and macro defects were grown successfully.

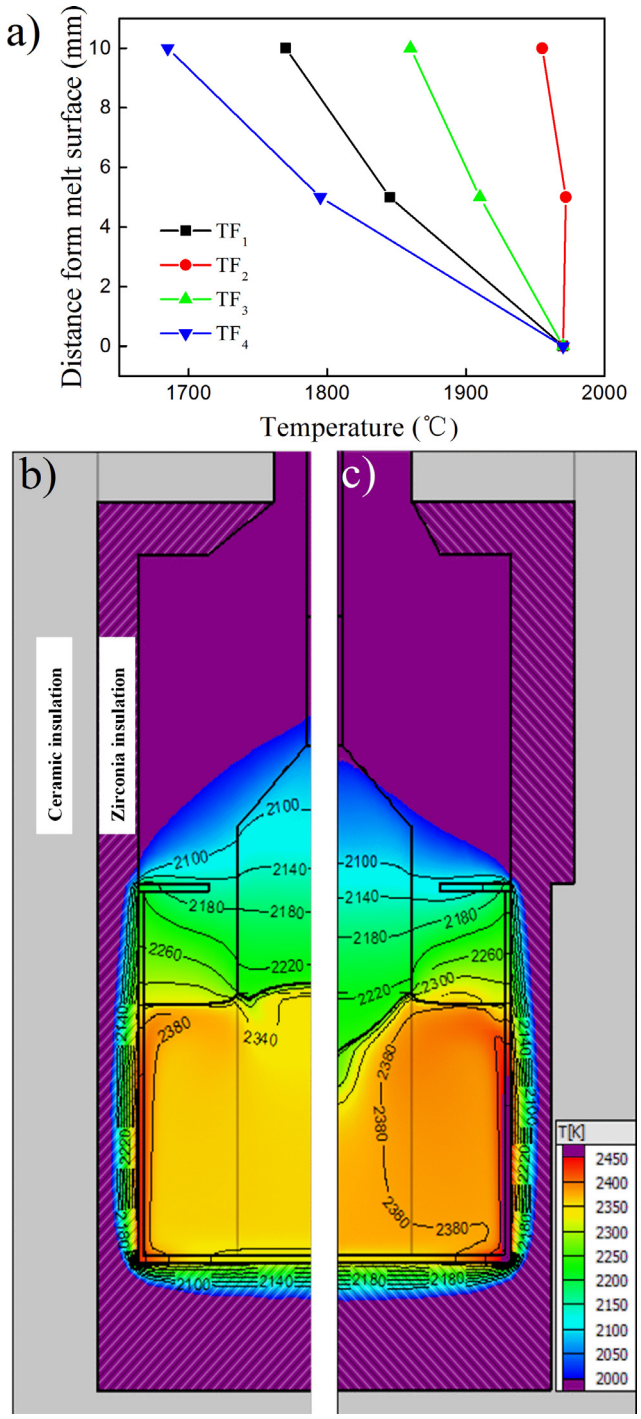

Fig. 4. (a) Temperature field (TF) of the melt surface at various conditions during crystal growth; the longitudinal axis represents the distance between the thermocouples and liquid. (b) and (c) Computer simulation results of the crystals growth temperature fields in the poor and modified temperature field, respectively. The multilayer zirconium oxide and ceramic materials were placed in a double-layer insulation structure.

As discussed above, after a series of adjustments, large-diameter Nd:YAG crystals were successfully grown (Fig. 6a). The crystal diameter, length of the cylindrical part, and the total length is 80 mm, 160 mm, and 400 mm, respectively. From Fig. 6a, it is clear that the as-grown Nd:YAG crystal possesses a perfect body control and crack-free structure with no bubbles or other macro defects. Furthermore, Fig. 6b and c present the internal structure

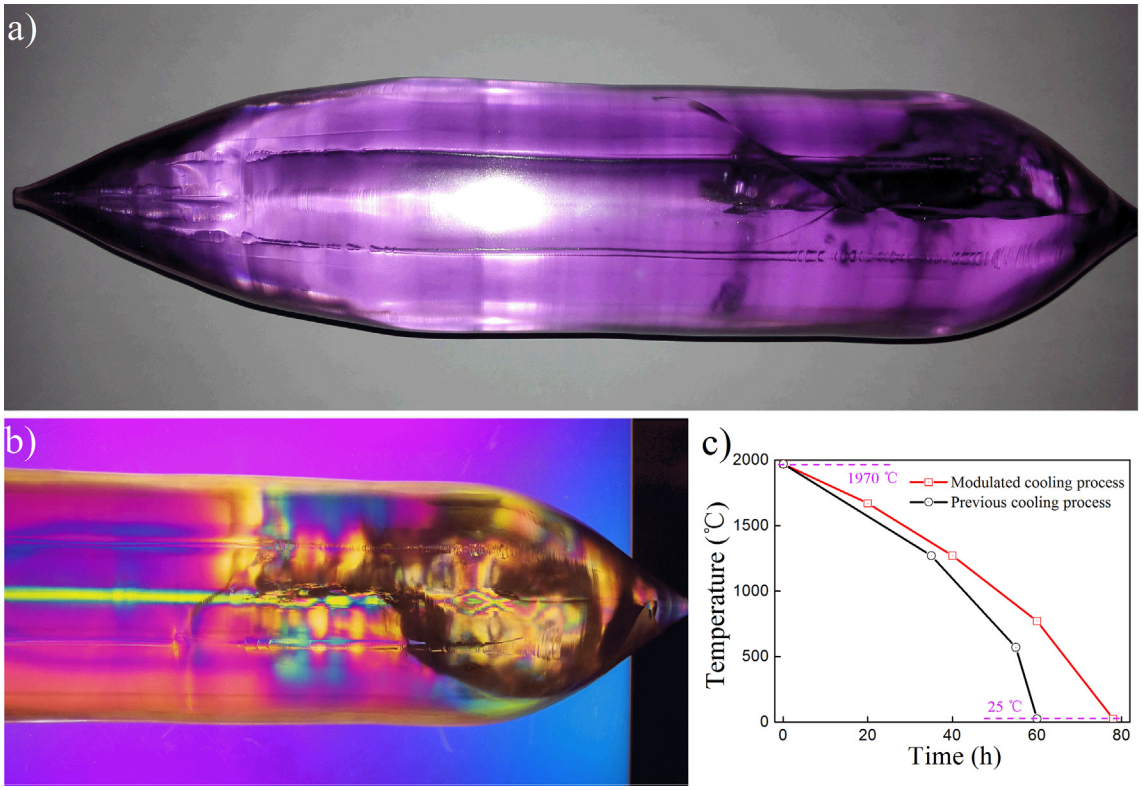

Fig. 5. (a) Tail cracking of the Nd:YAG crystal, and (b) the corresponding longitudinal parallel-plane polariscopic image. (c) Diagram of the cooling process before and after modification.

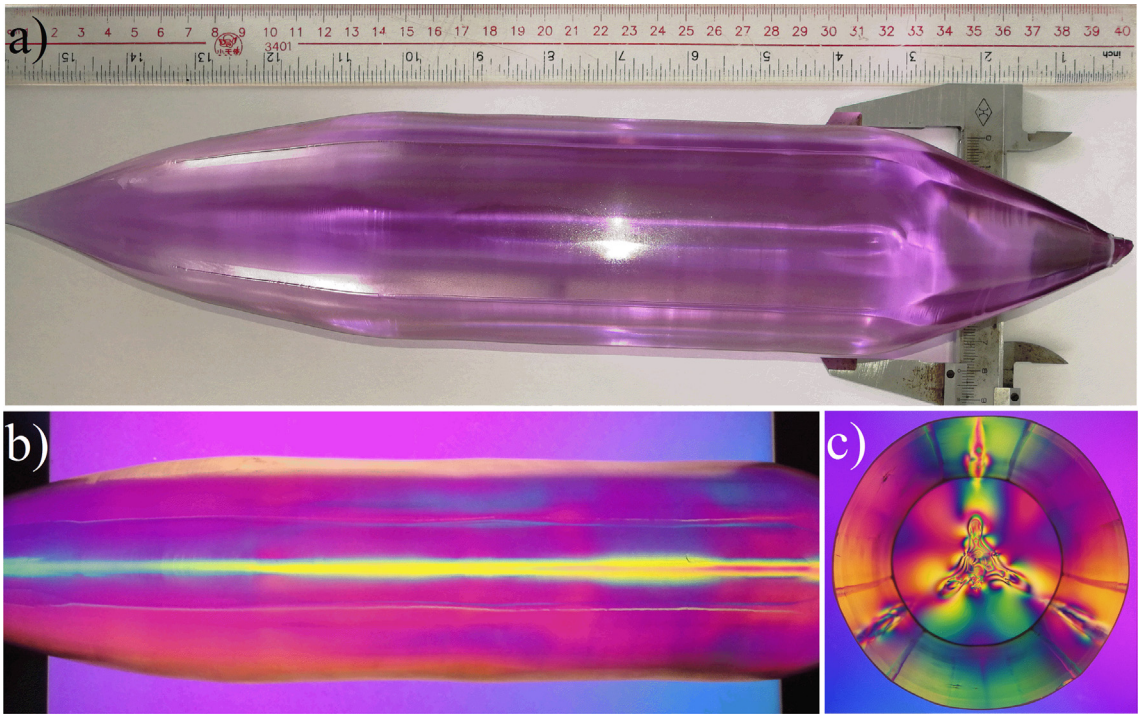

Fig. 6. (a) Large-diameter Nd:YAG crystal boule (diameter = 80 mm and total length = 400 mm). (b) The corresponding longitudinal parallel-plane polariscopic image. (c) Transverse parallel-plane polariscopic image from the end face of the as-grown crystal.

of the crystal cylinder from a parallel plane polariscope. No scattering particles are observed, and the area of the central and lateral core is small and homogeneous. Some rod samples, obtained via the cutting and rolling process, were selected to test the optical quality. Tables 2 and 3 show the test results of the crystal rods' extinction ratios and wavefront distortions. Different grades of

Table 2
Extinction ratio test of the different sizes of Nd:YAG rods.

Nd:YAG rods	Extinction ratio (dB)		
	Test values	Standard grade	Premium grade
Φ8 mm × 145 mm	30.4	≥22 dB	≥25 dB
Φ7 mm × 145 mm	31.5	≥22 dB	≥25 dB
Φ6 mm × 145 mm	32.8	≥22 dB	≥25 dB

Table 3
Wavefront distortion test of the different sizes of Nd:YAG rods.

Nd:YAG rods	Wavefront distortion (λ per inch @632.8 nm)		
	Test values	Standard grade	Premium grade
Φ8 mm × 145 mm	0.09	≤0.35	≤0.1
Φ7 mm × 145 mm	0.06	≤0.35	≤0.1
Φ6 mm × 145 mm	0.05	≤0.35	≤0.1

crystal rods have different optical quality standards. For example, when the crystal rod diameter is 6–8 mm, the standard grade of wavefront distortion and extinction ratio should be less than 0.35 λ and more than 22 dB, respectively; that of the premium-grade ones should be less than 0.1 λ and more than 25 dB, respectively. Therefore, we conclude that the as-grown Nd:YAG crystal has good optical qualities.

4. Conclusion

In summary, high-quality Nd:YAG crystals were successfully grown by the CZ method, and test results of the extinction ratio and wavefront distortion demonstrate that the crystal has good optical homogeneity. Four common defects of large-size Nd:YAG crystals were analyzed. The growth striations observed in the crystal surface were attributed to the unsuitable temperature field in the solid-liquid interface. Inclusions arose with the phenomenon of supercooling in the growth interface, the destroyed stability of the smooth interface, and the effect of fluctuating technology parameters. The comminuted crack formed in the shoulder process was attributed to the large temperature gradient that causes high heat stress and deformation. The temperature gradient above the melt was measured under various conditions during crystal growth; the experimental results indicate that a gradient of 25 °C/mm yields a high-quality Nd:YAG crystal. The results of the temperature field adjustment were also confirmed by computer simulation. In general, by adjusting the temperature field and optimizing the cooling procedure, large-size Nd:YAG crystals with a diameter of 80 mm and cylindrical part of 160 mm were grown successfully.

Acknowledgements

This work was supported by the National Natural Science Foundation of China (NSFC) (grant numbers 11372361, 11302268, 11232015, 11472321, 11572355); the National Natural Science Foundation of Guangdong province (2017A030310426); the Guangdong Science & Technology Project (grant number 2015B090927005); and the Fundamental Research Funds for the Central Universities (grant number 17lgpy37).

The authors would like to thank the Guangzhou Semiconductor Material Academy of Photoelectric Materials Research and Development Center for technical assistance in the crystal growth.

References

[1] M. Dunne, A high-power laser fusion facility for Europe, Nat. Phys. 2 (2006) 2–5.
[2] D. Naidoo, F.S. Roux, A. Dudley, et al., Controlled generation of higher-order Poincare sphere beams from a laser, Nat. Photon. 10 (2016) 327–332.
[3] C. Ambar, S.C. Vishwakarma, D.M. Vachhani, Ravindra Singh, Pushkar Misra, R. K. Jain, Study and development of 22 kW peak power fiber coupled short pulse Nd:YAG laser for cleaning applications, Opt. Laser Eng. 62 (2014) 69–79.
[4] H.M. Yang, G.Y. Feng, S.H. Zhou, Thermal effects in high-power Nd:YAG disk-type solid state, Opt. Laser Technol. 43 (2011) 1006–1015.
[5] L. Liu, X.B. Wang, S.F. Guo, H.Y. Li, Y.J. He, Unexpected temperature rise in end-pumped Nd^{3+}:YAG composite slab, Opt. Laser Technol. 44 (2012) 1738–1742.
[6] M. Katsurayama, Y. Anzai, A. Sugiyama, M. Kokie, Y. Kato, Growth of neodymium doped $Y_3Al_5O_{12}$ single crystals by double crucible method, J. Cryst. Growth 229 (2001) 193–198.
[7] M. Yadegari, M. Asadian, H. Saeedi, Y. Khodaei, N. Mirzaei, Formation of gaseous cavity defect during growth of Nd:YAG single crystals, J. Cryst. Growth 367 (2013) 57–61.
[8] K. Mazur, W. Wierzchowski, X-ray topographic investigation of growth defects and lattice parameter measurements within crystals of heavily neodymium doped yttrium aluminium garnet, J. Cryst. Growth 148 (1995) 345–354.
[9] R.F. Belt, R.C. Puttbach, D.A. Lepore, Crystal growth and perfection of large Nd: YAG single crystal, J. Cryst. Growth 13 (14) (1972) 268–271.
[10] K. Eunchong, C. Didier, K. Milan, S. Jennifer, Crystal growth of high doped Nd: YAG, Opt. Mater. 26 (2004) 337–341.
[11] S. Kostic, Z.Ž. Lazarevic, V. Radojevic, A. Milutinovic, et al., Study of structural and optical properties of YAG and Nd:YAG single crystals, Mate. Res. Bull. 63 (2015) 80–87.
[12] H. Saeedi, M. Yadegari, S. Enayati, et al., Thermal shocks influence on the growth process and optical quality of Nd: YAG crystal, J. Cryst. Growth 363 (2013) 171–175.
[13] O. Puncken, L. Winkelmann, M. Frede, et al., Heat generation in Nd:YAG at different doping levels, Appl. Optics 51 (2012) 7586–7590.
[14] D.E. Eakins, M. Held, M.G. Norton, D.F. Bahr, A study of fracture and defects in single crystal YAG, J. Cryst. Growth 267 (2004) 502–509.
[15] M. Gerber, T. Graf, Optimum parameters to etch Nd:YAG crystals with orthophosphoric acid H_3PO_4, Opt. Laser Technol. 33 (2001) 449–453.
[16] A. Lupei, C. Stoicescu, V. Lupei, X-ray and spectral characterization of defects in garnets, J. Cryst. Growth 177 (1997) 207–210.
[17] V. Iov, Characterization of garnet laser crystals by cathode luminescence emission in a scanning electron microscope, J. Cryst. Growth 167 (1996) 180–182.
[18] J.C. Brice, Study on crystal cracking, J. Cryst. Growth 42 (1977) 427–430.
[19] J. Banerjee, K. Muralidhar, Simulation of transport processes during Czochralski growth of YAG crystals, J. Cryst. Growth 286 (2006) 350–364.
[20] Y.Z. Zhu, D.C. Ma, S.W. Long, et al., In-situ detection of growth striations by crystallization electromotive force measurement during Czochralski crystal growth, J. Cryst. Growth 475 (2017) 70–76.
[21] C. Stelian, A. Nehari, I. Lasloudji, et al., Modeling the effect of crystal and crucible rotation on the interface shape in Czochralski growth of piezoelectric langatate crystals, J. Cryst. Growth 475 (2017) 368–377.
[22] Y. Okano, T. Fukuda, A. Hirata, et al., Numerical study on Czochralski growth of oxide single crystals, J. Cryst. Growth 109 (1991) 94–98.
[23] J.H. Jeong, I.S. Kang, Analytical studies on the crystal-melt interface shape in the Czochralski process for oxide single crystals, J. Cryst. Growth 218 (2000) 294–312.
[24] Z. Mingfu, G. Huaixin, H. Jiecai, et al., Distribution of neodymium and properties of Nd:YAG crystal by horizontal directional solidification, J. Cryst. Growth 340 (2012) 130–134.
[25] H.S. Fang, J.Z. Lin, L.L. Zheng, X.M. Huang, Analysis and optimization of Czochralski laser oxide crystal growth, Int. J. Heat Mass. 85 (2015) 505–512.